JOURNAL OF APPLIED GEOSPATIAL INFORMATION

Vol 10 No 1 2026

http://jurnal.polibatam.ac.id/index.php/JAGI
ISSN Online: 2579-3608

Numerical Modeling Analysis of Tsunami Inundation in the Coastal Area of Ngadirojo, Pacitan Regency

Muhamad Rakif Panguale [1,*], Muhammad Fiky Izzulhaq[2], Chezta Ahmad Muzakky[2]

[1] Shipbuilding Engineering, Shipbuilding Institute of Polytechnic Surabaya, Surabaya, Indonesia
[2] Marine Engineering, Shipbuilding Institute of Polytechnic Surabaya, Surabaya, Indonesia
*Corresponding author e-mail: muhamad.rakif@ppns.ac.id

Received: May, 18 2026
Accepted: June 28, 2026
Published: June 30, 2026

Abstract

Coastal communities along the southern coast of Java are increasingly vulnerable to tsunami hazards due to active seismotectonic conditions in the Indian Ocean. This study presents a comprehensive numerical modeling analysis of the tsunami inundation map in the Ngadirojo coastal area of Ngadirojo Subdistrict, Pacitan Regency, East Java. The research objectives are to simulate potential tsunami scenarios, map inundation extents, and assess coastal vulnerability for disaster risk reduction planning. The Cornell Multi-grid Coupled Tsunami Model (COMCOT) is employed to simulate tsunami propagation and coastal inundation using high-resolution bathymetric and topographic data. The modeling incorporates nested grid systems with spatial resolutions ranging from 1250 m in deep ocean to 10 m in nearshore areas. The study provides a detailed analysis using numerical modeling techniques for predicting tsunami wave heights, inundation distances, and arrival times with a single earthquake source scenario of maximum magnitude Mw 8.8 in the Pacitan coastal region. Results indicate that tsunami waves could reach a maximum height of 16.4 m, with inundation extending up to 3.98 km inland and arrival times as short as 30 minutes. The derived tsunami hazard index highlights extensive high-risk zones along Soge and Taman Ngadirojo Beaches. The study provides essential scientific data to help local authorities develop effective evacuation strategies, early warning systems, and coastal protection measures, and significantly contributes to tsunami risk assessment methodologies for similar coastal environments in Indonesia and the Indo-Pacific region.

Keywords: COMCOT, inundation, Ngadirojo, numerical modeling, tsunami

1. Introduction

Tsunamis are among the most destructive natural disasters threatening coastal communities worldwide (Handayani et al., 2022; Dias et al., 2024). Indonesia, located in the Pacific Ring of Fire and at the convergence of three major tectonic plates (the Eurasian, Indo-Australian, and Pacific Plates), is highly vulnerable to tsunamis due to its extensive coastline and high level of seismic activity (Setyaningsih et al., 2023; Jumadi et al., 2025). Most tsunamis in Indonesia are triggered by shallow megathrust earthquakes in subduction zones, where one tectonic plate is forced beneath another, causing large vertical displacements of the seafloor (Hamza et al., 2000). Historical records show that between 1600 and 2007, 109 tsunamis occurred in Indonesia, with approximately 90% of them caused by tectonic earthquakes (Triyono et al., 2019).

The southern coast of Java, including Pacitan Regency, is one of the regions with the highest tsunami risk (Supendi et al., 2023). This area is adjacent to the East Java Megathrust, a segment of approximately 440 km with a slip rate of up to 4 cm per year, indicating significant tectonic energy accumulation (Widiyantoro et al., 2020). Several studies have identified seismic gaps in this zone, particularly from Central Java to East Java, that have not released major earthquakes for decades. This condition suggests the potential for a large-magnitude earthquake, possibly up to Mw 8.8, capable of generating tsunamis with run-up heights of up to 20 meters in some coastal areas (Horspool et al., 2014; Widiyantoro et al., 2020). Historical evidence, in the form of paleotsunami deposits found in Pacitan and Trenggalek, further confirms the recurrence of tsunami events in this region (Anugrah *et al.,*2015). From a geomorphological perspective, the coastal area of Ngadirojo District in Pacitan Regency is highly vulnerable due to its low-lying coastline, the presence of river mouths, and dense coastal settlements. These conditions enhance the potential for tsunami waves to penetrate further inland, thereby amplifying disaster risk for local communities (Wibowo et al., 2023; Jumadi et al., 2025). Therefore, accurate tsunami inundation mapping is crucial not only for disaster risk assessment but also as a basis for evacuation planning, spatial development, and the construction of disaster-resilient coastal infrastructure (Sutoyo & Syafiudin, 2024)

In developing tsunami inundation maps, numerical modeling plays a crucial role in simulating the propagation of tsunami waves from their seismic source to the coastal regions (Widodo et al., 2024). The simulations are performed using the Cornell Multi-grid Coupled Tsunami (COMCOT) model (Liu & Wang, 2011). This model solves the long-wave equations in shallow water conditions and transforms seismic source parameters into spatially distributed tsunami propagation, run-up, and inundation statistics. The shallow water equations are widely adopted in tsunami modeling due to their computational efficiency and their suitability for representing long-wave dynamics (Triono et al., 2019).

The accuracy of tsunami inundation simulations is strongly influenced by the representation of topography and land-surface characteristics within the model. Therefore, this study utilizes the Forest and Buildings Removed Copernicus DEM (FABDEM) and DeltaDTM, which were developed to provide improved representations of bare-earth terrain through the correction of vegetation, building, and other surface-object effects (Hawker et al., 2022; Pronk et al., 2024). A realistic representation of coastal topography is essential for tsunami modeling because it affects wave propagation, run-up, and inundation patterns in coastal areas. In addition, the influence of surface roughness (bottom friction) is incorporated through Manning's roughness coefficients derived from land-cover data, allowing variations in flow resistance associated with built-up areas, vegetation, open land, and water bodies to be represented within the simulations (Dyakonova and Khoperskov, 2018). The integration of improved terrain representation and land-cover-based bottom friction is expected to enhance the realism of tsunami inundation processes and provide hazard information that more closely reflects actual coastal conditions in Ngadirojo District.

In this study, tsunami scenarios were generated based on the potential South Java Megathrust earthquake as proposed by Widyantoro (2020). The numerical modeling results were subsequently integrated into the development of tsunami hazard maps and hazard indices to translate complex quantitative outputs into practical indicators of tsunami risk. The hazard index simplifies model results into operational information that can be effectively utilized for evacuation route planning, disaster mitigation strategies, and risk-based coastal development at the local scale (Horspool et al., 2014).

Beyond inundation mapping, information on tsunami hazard classes is a critical component of coastal disaster risk management. Numerical parameters such as wave height, inundation depth, and inundation distance are highly technical and difficult to interpret directly. Therefore, hazard levels need to be classified into low, medium, and high categories. This classification enables rapid identification of high-risk areas, supports the prioritization of evacuation planning, risk-based coastal spatial planning, and informed decision-making during the pre-disaster phase, including the designation of no-build zones and the strengthening of risk communication through early warning systems (Merz et al., 2020). This classification also serves as a foundation for developing more effective and responsive tsunami mitigation strategies (Benazir & Oktari, 2024) and can further facilitate more efficient emergency response and post-tsunami recovery (Satake, 2014).

The objective of this research is to analyze tsunami inundation in the coastal area of Ngadirojo District, Pacitan Regency, through numerical modeling using the COMCOT model. Specifically, the study aims to: (1) evaluate the influence of terrain representation based on FABDEM and DeltaDTM, as well as land-cover-based bottom friction, on the simulation of tsunami propagation, run-up, and inundation generated by a South Java Megathrust earthquake scenario; (2) produce high-resolution tsunami hazard maps for the study area; and (3) develop tsunami hazard classifications based on modeled tsunami inundation to support the preparation of tsunami hazard maps for disaster risk reduction, evacuation planning, and coastal spatial management.

2. Method

The research activities conducted in this study consisted of two main stage. The first stage involves the numerical modeling of tsunamis using the COMCOT 1.7 model, which produces outputs in the form of tsunami inundation, tsunami run-up, and tsunami arrival time. These outputs provide the physical basis for understanding the potential impacts of tsunamis in the study area. In the second stage, the inundation results are further analyzed to derive a tsunami hazard index and corresponding hazard classes. This study enables the transformation of numerical outputs into practical indicators that can be directly applied to disaster risk assessment and spatial planning. The research flowchart adopted in this study, from tsunami modelling to tsunami hazard classification, is presented in Figure 1.

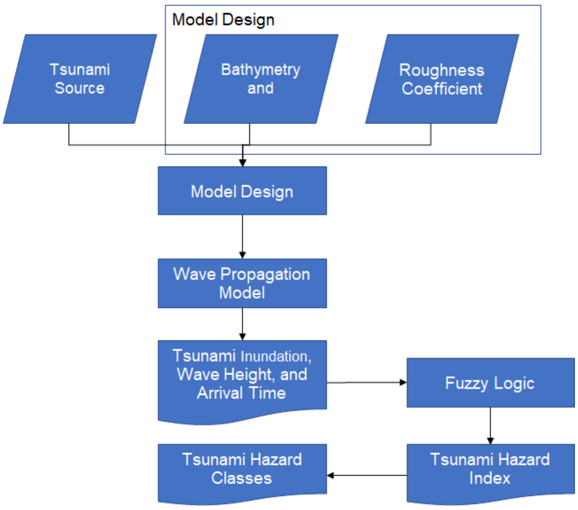

Figure 1. Research Flowchart

The topography data used in this study is the Digital Elevation Model (DEM). DEM datasets applied in this study include FABDEM (Forest and Buildings removed Copernicus DEM) and DeltaDTM (Digital Terrain Model), both of which provide essential topographic detail for accurate tsunami modeling. The choice of DEM datasets is crucial, as they play a key role in capturing water level variations during inundation. FABDEM is used to represent terrain above 10 meters, offering higher accuracy than many other global datasets (Marsh *et al*., 2023; Osama *et al.,* 2023). Its improved spatial resolution also allows the identification of fine-scale features, such as narrow drainage channels, making it particularly valuable for tsunami hazard mapping. In contrast, DeltaDTM is applied to elevations between 0 and 10 meters, optimized for coastal and low-lying areas (Pronk *et al.,* 2024). These datasets are subsequently integrated to construct a comprehensive elevation model of the study area.

Bathymetry data were obtained from the Indonesian National Bathymetry dataset (BATNAS) with a spatial resolution of approximately 6 arc-seconds (≈180 m) and were referenced to the mean sea level (MSL) datum (Arafat et al., 2025). These data provide essential information on the seafloor's depth and morphology that critically influences wave tsunami propagation and inundation simulations (Windupranata et al., 2025). High-quality bathymetry such as BATNAS has been demonstrated to significantly enhance the representation of the marine domain in tsunami hazard studies, allowing the model to more accurately capture wave transformation and propagation patterns over continental slopes and nearshore zones, an aspect confirmed in recent tsunami analyses that integrate BATNAS as the primary bathymetric input for numerical modeling domains.

The tsunami-generated earthquake parameters applied in this study are derived from the East Java Megathrust, which is estimated to have the potential to generate a maximum magnitude of Mw 8.8 (Widyantoro et al., 2020). This scenario represents the worst-case earthquake event that may occur in the East Java megathrust. The tsunami source is modeled as a multifault scenario, considering the possible interactions of several fault segments within the megathrust that could rupture simultaneously. The detailed parameters of the tsunami-generated earthquake are presented in Table 1.

Land cover data provided by BIG (Geospatial Information Agency) are used to classify the types of land cover along the coastline and adjacent areas. These datasets are used to determine roughness coefficients, which are essential in representing the reduction of water flow velocity through frictional resistance over different surface types. Within the framework of tsunami modeling, higher roughness coefficient values decrease wave velocity and flow energy, thereby limiting the extent and distance of inundation (Kaiser et al., 2011; Cárdenas and Catalán, 2022). As a result, areas characterized by high surface roughness, such as forested zones or densely built environments, can function as natural barriers that obstruct tsunami flow propagation (Gibbons et al., 2022; Li et al., 2025). Table 2 presents Manning's roughness coefficients applied in this study.

Table 1. Parameters of worst-case tsunami-negated earthquake [7]

Epicenter		Dimension (m)		Focal Depth (m)	Focal Mechanism (o)			Dislocation (m)	Mag (Mw)
Latitude	Longitude	Length	Width		Strike	Dip	Lake		
-9.73681	110.1249	150000	91000	18000	278	16	90	14.3	
-9.92469	111.4618	150000	91000	18000	278	16	90	11.3	8,8
-10.11126	112.7987	150000	91000	18000	278	16	90	14.6	

Table 2. Manning's roughness coefficient for each land use

Land Use	Manning's coefficient
Oceans, Rivers	0.013
Pavement ground (industrial area, township/city, Road)	0.015
Arable land (including waste land, open field)	0.016-0.022
Woodland (e.g., orchard, grass, bushes, low density forest, farm)	0.025-0.027
Low density residential areas (density <30%)	0.028
Mid density residential areas (density 30-50%)	0.03
High density residential areas (density >50%)	0.032
Buildings (residential/industrials)	0.2

2.1 Numerical Modeling

The numerical simulations were conducted using the COMCOT model. The governing equations of COMCOT are based on the conservation of mass and momentum expressed in flux form. The numerical method uses the leapfrog method (explicit leapfrog finite difference method). This numerical scheme counts time and space with the second order of the central difference equation. It means that the water level is calculated in the middle of the grid cell, while the flux is calculated on the sides of each grid cell based on the COMCOT manual (Wang, 2009).

In COMCOT, the fundamental governing equation is a discussion of the mass-momentum equations in terms of fluxes. The linear terms from the governing equations are adequate for the tsunami's deep-water propagation. The following equations (2) and (3) in Cartesian coordinates can be used to solve the two-dimensional problems:

$$\frac{\partial \eta}{\partial t} + \left\{\frac{\partial P}{\partial x} + \frac{\partial Q}{\partial y}\right\} = -\frac{dh}{dt}$$

$$\frac{\partial P}{\partial t} + gh\frac{\partial \eta}{\partial x} - fQ = 0$$

$$\frac{\partial Q}{\partial t} + gh\frac{\partial \eta}{\partial y} + fP = 0$$

In the same way, the governing equations with nonlinear terms in Cartesian coordinates' area:

$$\frac{\partial \eta}{\partial t} + \left\{\frac{\partial P}{\partial x} + \frac{\partial Q}{\partial y}\right\} = -\frac{dh}{dt}$$

$$\frac{\partial P}{\partial t} + \frac{\partial}{\partial x}\left(\frac{P^2}{H}\right) + \frac{\partial}{\partial x}\left(\frac{PQ}{H}\right) + gH\frac{\partial \eta}{\partial x} + F_x = 0$$

$$\frac{\partial P}{\partial t} + \frac{\partial}{\partial x}\left(\frac{PQ}{H}\right) + \frac{\partial}{\partial x}\left(\frac{P^2}{H}\right) + gH\frac{\partial \eta}{\partial y} + F_x = 0$$

The value of F represents the subsurface friction in the X and Y directions, which is written in equations (7) and (8):

$$F_x = \frac{gn^2}{H^{\frac{7}{3}}} P(P^2 + Q^2)^{1/2}$$

$$F_y = \frac{gn^2}{H^{\frac{7}{3}}} Q(P^2 + Q^2)^{1/2}$$

Where:

g : gravity acceleration [m/s^2]
P : flux discharge in x-direction (W–E) [m/s^2]
Q : flux discharge in y-direction (S–N) [m/s^2]
f : Coriolis force coefficient [-]
R : radius of the Earth [m]
h : water depth [m]
η : water surface elevation [m]
H : total water depth [m]
F_x, F_y : bottom friction in x and y direction
n : Manning roughness coefficient [s/m$^{1/3}$]
u : current velocity in x direction [m/s]
v : current velocity in y direction [m/s]

2.2 Tsunami Hazard Level

The tsunami hazard index represents a transformation of the estimated tsunami height into numerical values ranging from 0 to 1. Higher tsunami wave heights (greater than 3 meters) yield index values approaching 1, whereas lower heights (less than 1 meter) result in values closer to 0. This transformation is carried out using a fuzzy logic approach. The inundation depth values obtained from tsunami modeling are converted from meters into hazard indices, which are then categorized according to the BNPB Regulation No. 2 of 2012, as presented in Table 3. Based on this classification, the exposed areas can be grouped into three hazard levels, low, medium, and high, derived from the tsunami height values generated in the previous inundation modeling.

Table 3. Range of Inundation Height and Hazard Index Based on Hazard Level (BNPB, 2018)

Classes	Inundation	Index
Low	≤ 1	0-0.333
Middle	1 < inundation ≤ 3	0.334-0.666
High	> 3	0.667-1

3. Result and Discussion

3.1 Simulation Setting

Tsunami modeling requires a consistent integration of terrestrial topographic data and marine bathymetric data. Bathymetric data provide information on seafloor depth, while topographic data describe land elevation. Without proper integration, inconsistencies may arise along the shoreline boundary, which can significantly reduce the accuracy of tsunami propagation and inundation simulation (Ayunda et al*.,* 2020). To address this issue, a preprocessing stage was conducted to harmonize the vertical and horizontal references of all datasets, resulting in a continuous elevation surface extending from the deep ocean to coastal land areas. During this process, bathymetric and topographic datasets were merged through mosaicking and spatial correction procedures, producing an integrated elevation model with a high level of consistency across the study area.

In the integration process, bathymetric values were retained only for elevations below 0 m, representing underwater depths, while topographic values were retained for elevations above 0 m, representing land elevations. Elevation data at 0 m, corresponding to the shoreline, were derived from the Indonesian Topographic Base Map (RBI). Through this integration, a seamless elevation dataset was produced in which positive elevation values indicate land areas and negative values represent marine areas. The final integrated dataset has a spatial resolution of 10 m and serves as the fundamental basis for constructing the computational grids used as input for tsunami numerical simulations. Figure 2 illustrates the bathymetric data, topographic data, and the integrated dataset prepared for numerical modeling.

The grid configuration in COMCOT adopts the nested grid approach, which allows multi-scale analysis from global to local domains. This approach allows detailed grids to be used only in the specific area of interest, thereby optimizing computational efficiency. The main advantage of this method is that it significantly reduces simulation time while maintaining accuracy and minimizing the risk of numerical errors. Coarse parent grids are used to simulate wave propagation in deep waters, while progressively finer child grids capture detailed wave dynamics nearshore. Nested Grid Configuration makes it possible to obtain more detailed information on coastal areas by using a finer grid (Chau et al., 2015).

In this study, four nested grid layers were constructed based on the integration of bathymetric and topographic datasets, each with different spatial resolutions. Layer 1 represented the Indian Ocean using BATNAS data at a coarse resolution of 1250 m; Layer 2 refined the domain toward southern Java and Pacitan waters with a medium resolution of 250 m; Layer 3 further increased the detail with 50 m resolution; and Layer 4 employed the high-resolution integrated topography–bathymetry dataset at 10 m for detailed coastal inundation analysis at the sub-district level. This multi-layer grid system ensures computational efficiency while maintaining accuracy at local scales. Coarse grids effectively describe tsunami propagation in deep water, whereas fine-resolution grids are crucial for determining inundation depth, run-up, and inland penetration distances. Consequently, the modeling results provide reliable and site-specific information to support tsunami hazard assessment and disaster risk mitigation planning. Figure 3 shows the domain model in this study using a nested grid.

The tectonic source to generate the tsunami scenario originates from the Java Megathrust source, specifically the East Java segment, using a multifault scenario. This scenario considers the potential interaction of multiple fault segments within the megathrust system that may rupture simultaneously. The scenario (Table 1) represents the worst-case earthquake event that may occur in the East Java megathrust with Mw 8.8 (Widyantoro et al., 2020). Figure 3 shows the tectonic source from the study area. The black rectangular outline represents the megathrust source area of the Indo-Australian subduction zone. The red lines and red boxes indicate the segmentation of the megathrust earthquake source used in the numerical simulations. Meanwhile, the color gradient ranging from red to green is produced by the tsunami generation model, representing the initial tsunami height resulting from seabed deformation along the East Java–Sumba Thrust segment, which is used as the tsunami source.

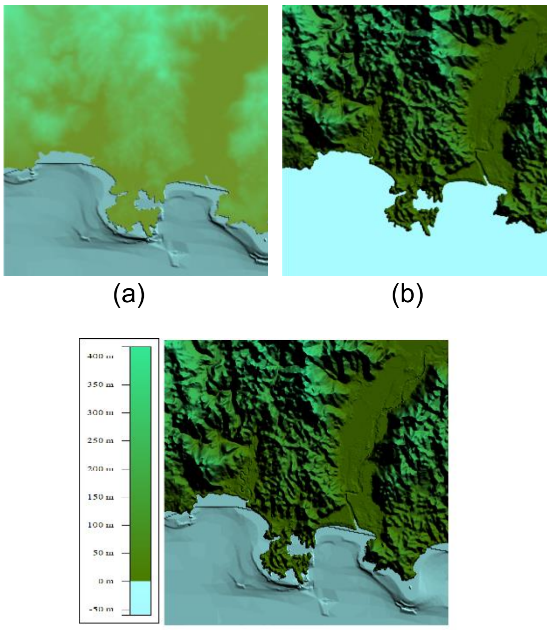

(a) (b)

(c)

Figure 2. Topography data (a), bathymetry data (b), and data assimilation of both topography and bathymetry

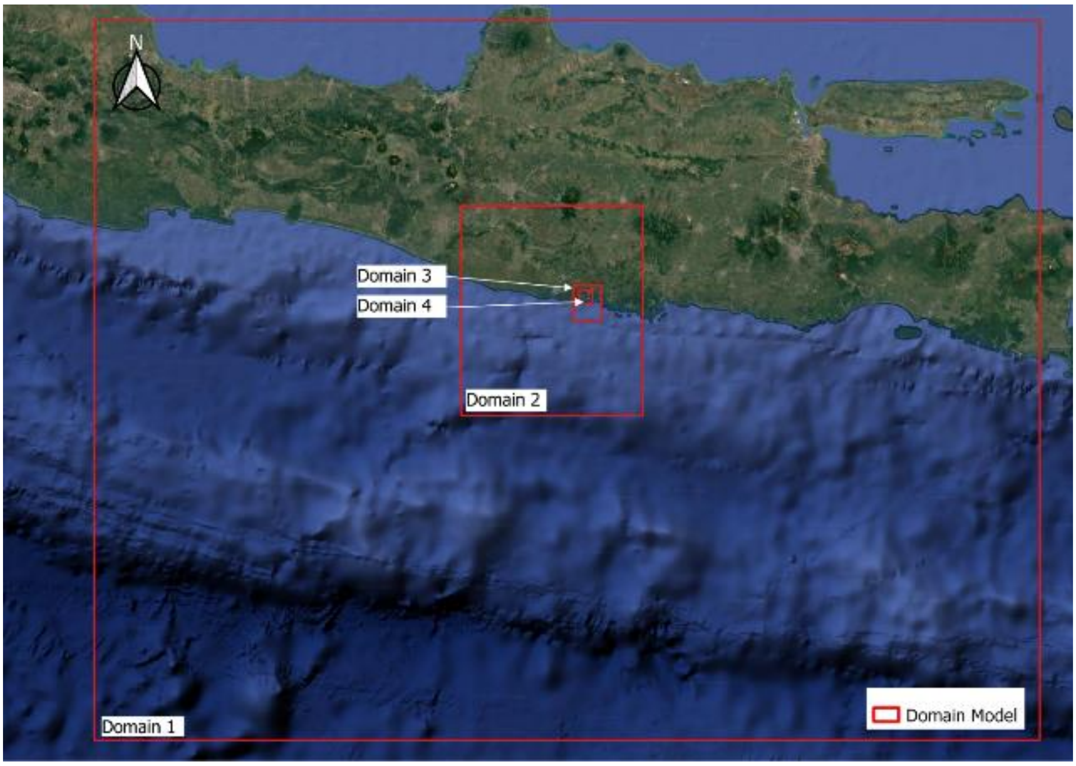

Figure 3. Model domain using nested grid

3.2 Tsunami Numerical Model

Vertical deformation of the seafloor caused by megathrust earthquakes is the primary mechanism responsible for tsunami generation. When the seafloor undergoes sudden uplift or subsidence, the overlying water mass is displaced, resulting in the formation of an initial tsunami condition (Saito, 2013). The magnitude of sea surface deformation is controlled not only by the amount of seabed displacement but also by the rate of deformation. Faster deformation transfers greater energy from the seafloor to the water column, producing higher ocean-bottom pressure, stronger flow velocities, and larger tsunami amplitudes. In addition, tsunami wave characteristics are strongly influenced by earthquake source parameters, including source depth, strike direction, and the surrounding bathymetric morphology along the tsunami propagation path.

Figure 4 illustrates the earthquake source parameters derived from the initial tsunami generation conditions associated with the Indo-Australian subduction zone. The tsunami scenario was generated from a potential megathrust earthquake in the southern waters of East Java with a maximum estimated magnitude of Mw 8.8, located approximately 440 km from the study area. This scenario was selected as a worst-case event because of its potential to produce severe impacts along the coastal area of Pacitan Regency. The earthquake source was modeled as a multifault rupture, assuming that several megathrust segments ruptured simultaneously, thereby generating larger vertical seabed deformation. The deformation pattern reflects opposite crustal movements, where positive values indicate rapid uplift and negative values indicate subsidence. Such abrupt vertical deformation displaced the overlying water mass and generated significant sea surface fluctuations from the seabed to the ocean surface. Shallow earthquake sources with large energy release tend to produce greater vertical displacement contrasts, resulting in stronger tsunami wave generation (Newman and Okal, 1998; Geist, 2020).

The simulation results indicate that the initial tsunami condition produced sea surface elevation changes due to vertical seafloor deformation following the megathrust earthquake. Positive values represent uplift of the oceanic crust, whereas negative values indicate subsidence. These results are consistent with tsunami generation theory, which states that sudden seafloor deformation displaces the water mass from the seabed to the sea surface and acts as the primary source of tsunami wave formation. Variations in vertical displacement among the earthquake source scenarios reflect differences in energy transfer from crustal deformation to the water column, resulting in different initial tsunami characteristics for each simulation scenario. When the oceanic plate undergoes uplift following megathrust rupture, large volumes of water are forced upward, initiating tsunami propagation.

In addition to earthquake-induced deformation, tsunami propagation is also affected by shoaling processes and wave dispersion characteristics. In near-field tsunami regions, the shallow-water theory approach remains sufficiently representative because dispersive effects are relatively small. However, as tsunami waves propagate toward shallower coastal waters along the southern coast of Java, wave amplitudes increase due to the shoaling effect (Glimsdal et al., 2013; Aditama et al., 2023). The three selected earthquake source points were oriented toward the southern coast of Java. The strike direction of the tectonic sources toward the southern coast of Java enhances the concentration of tsunami energy toward the coastline. Consequently, tsunami waves experience greater amplification in shallow coastal waters compared to propagation toward deeper offshore regions. Fault strikes directed toward shallower bathymetric features generated higher tsunami waves because of stronger shoaling amplification, whereas fault orientations towards deeper bathymetric regions produced relatively smaller waves. Therefore, the simulated initial condition not only represents the initial sea surface deformation generated by the earthquake but also describes the dynamic energy transfer and tsunami propagation processes toward the Pacitan coastal area, which are influenced by both earthquake source characteristics and regional bathymetric morphology.

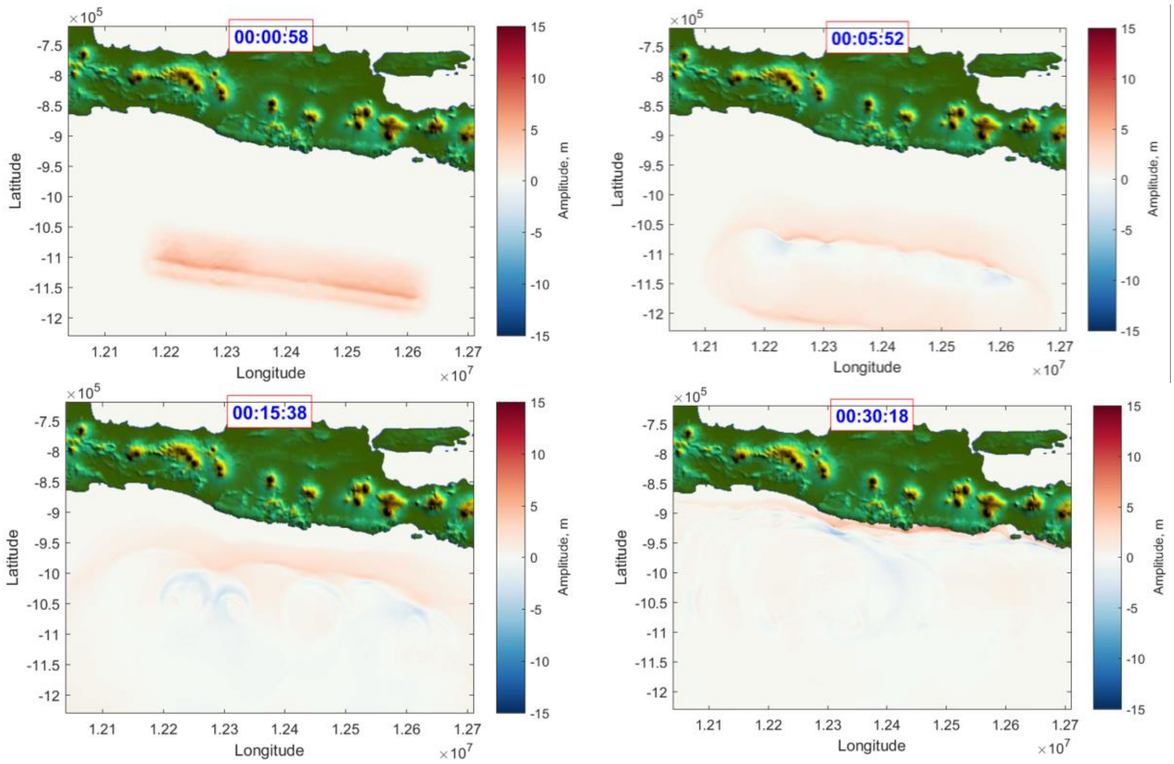

Figure 4. Temporal simulation at layer 1 at 0, 5, 15, and 30 minutes

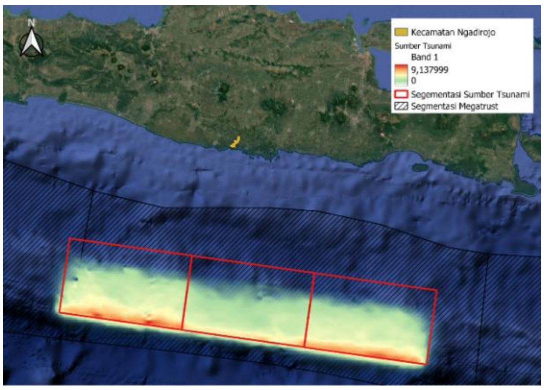

Figure 5. Initial condition

The tsunami propagation simulation was conducted over a 90-minute period to analyze the temporal evolution of tsunami waves from the offshore source region toward the coastal area of Pacitan Regency. At minute 0, immediately after the earthquake occurred, seafloor deformation generated uplift and subsidence around the fault plane, forming an initial sea surface disturbance characterized by a dipole pattern. Positive elevations developed in uplifted areas, whereas negative depressions formed in subsided regions.

At minute 5, tsunami waves remained concentrated around the epicentral area. By minute 15, tsunami energy had propagated toward the southern coast of Java, while wave amplitudes gradually decreased due to radial energy dispersion during offshore propagation. At minute 29, tsunami waves began reaching the Ngadirojo coastal area and experienced wave amplification due to shoaling processes as they entered shallow waters (Tonegawa and Fukao, 2022). By minute 30, part of the tsunami waves had already inundated coastal inland areas. Figure 5 illustrates the tsunami propagation patterns at 0, 5, 15, and 29 minutes after the earthquake event.

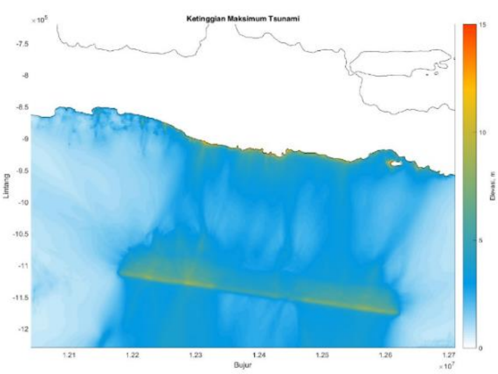

Figure 6. Tsunami Amplitude

Tsunami propagation was modeled using the explicit leapfrog finite difference scheme within the COMCOT framework to solve the nonlinear shallow water equations under complex bathymetric conditions. The simulation results indicate that the maximum offshore tsunami amplitude reached approximately 33 m before approaching the coastline, with an average arrival time of about 30 minutes. (Figure 6 and Figure 7). As tsunami waves propagated into shallow coastal waters, wave transformation processes became increasingly significant due to variations in water depth and seabed morphology.

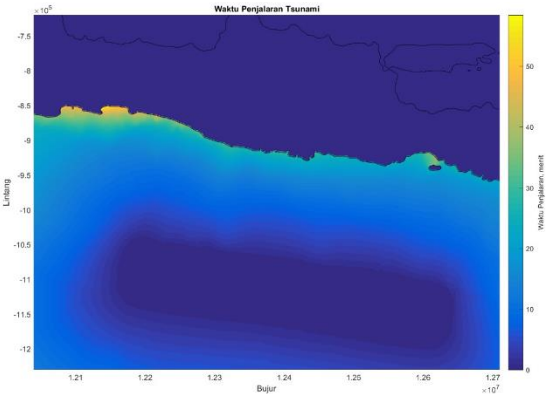

Figure 7. Tsunami Time Travel

In addition to shoaling, refraction and resonance processes also influenced tsunami wave behavior in coastal areas. Refraction caused by variations in seabed slope altered the propagation direction of tsunami waves, concentrating tsunami energy along specific coastal segments, particularly around bays and headlands. Meanwhile, resonance within semi-enclosed bays amplified wave heights through the interaction between incoming and reflected tsunami waves (Pakoksung et al., 2023; Cheng et al., 2023). These combined processes resulted in spatial variations in tsunami intensity along the southern coast of Ngadirojo Subdistrict and increased tsunami hazard potential in bay-shaped coastal regions.

A more detailed tsunami inundation analysis was conducted using the layer 4 simulation domain representing the district-scale area. The COMCOT output parameter hmax_layerxx was used to describe the maximum sea surface elevation during tsunami propagation. In this study, tsunami inundation was defined as the maximum horizontal penetration distance of tsunami waves inland from the coastline, while run-up referred to the maximum vertical elevation reached by the tsunami above mean sea level in coastal areas. Simulation visualization showed that tsunami waves began approaching the Ngadirojo coastline at minute 29, while at minute 30, the tsunami had already inundated inland areas within Ngadirojo Village. Figure 8 presents the temporal simulation results for layer 4 at 30, 37, 40, and 70 minutes after the earthquake.

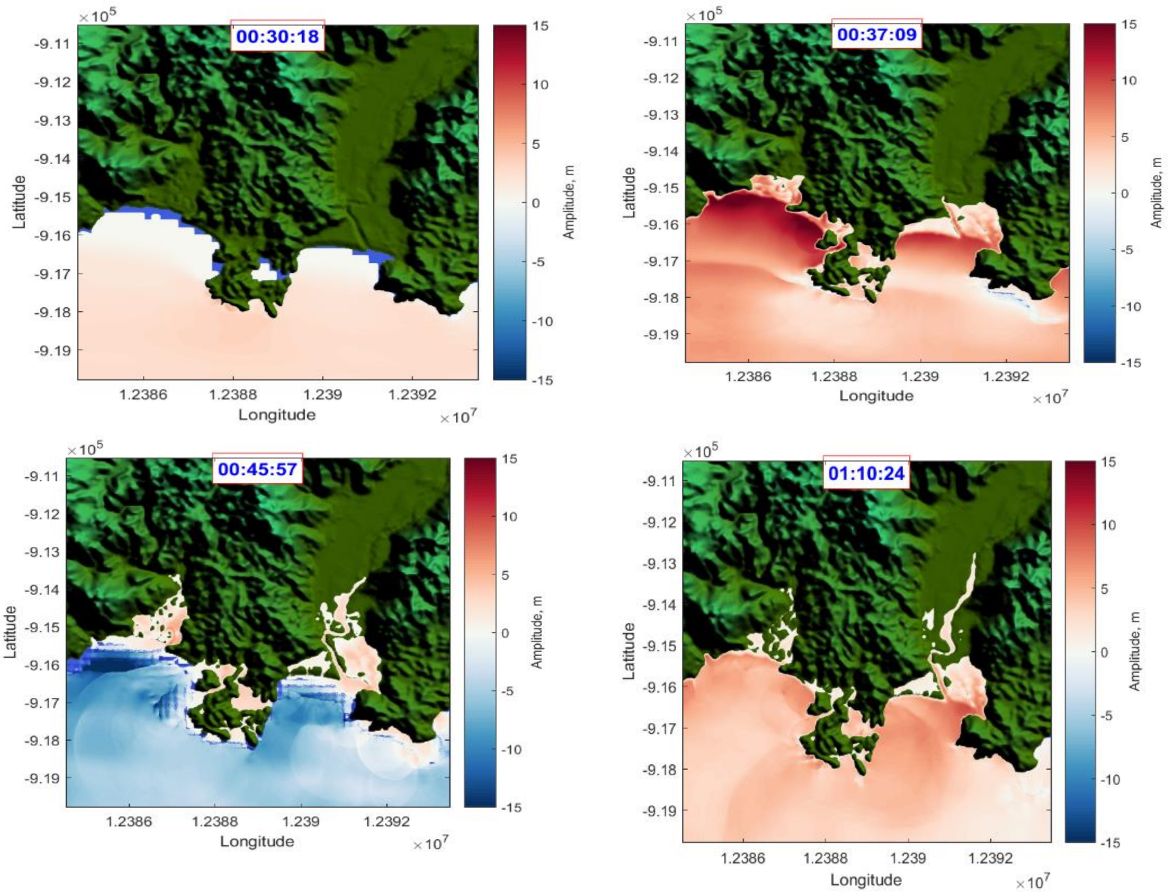

Figure 8. Temporal simulation at layer 4

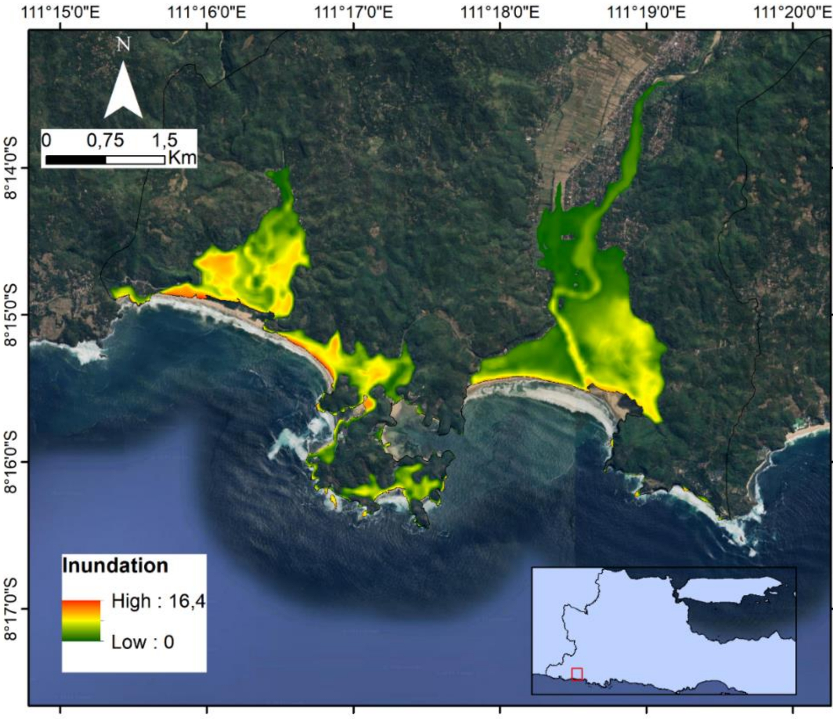

Figure 9. Tsunami Inundation and run-up at the study area

To further evaluate tsunami characteristics, virtual tide gauge analysis was applied at several observation points along the coastline (Figure 10). The virtual tide gauge results showed variations in tsunami wave heights, with maximum wave heights reaching approximately 16.21 m and tsunami arrival times ranging between 29 and 33 minutes after the earthquake (Figure 11). This relatively short arrival time indicates the characteristics of a near-field tsunami, where waves reach coastal regions rapidly and increase the vulnerability of coastal communities to tsunami hazards (Chen et al., 2023). These conditions also emphasize the importance of tsunami early warning systems and rapid inundation estimation to support coastal disaster mitigation efforts (Núñez et al., 2022). Figure 8 presents the virtual tide gauge results at several observation points. Overall, the simulation results demonstrate that tsunami hazard levels in Ngadirojo Subdistrict are strongly influenced by the interaction between earthquake source characteristics, tsunami propagation dynamics, coastal morphology, and nearshore bathymetric conditions.

The maximum tsunami inundation distance of approximately 3.98 km and the maximum run-up height of 16.4 m obtained in this study are lower thanthose reported by Aditama et al. (2023) and Widodo et al. (2023) for the Pacitan coastal region. Previous studies generally reported larger inundation extents and higher run-up values under South Java megathrust earthquake scenarios, indicating that tsunami impact estimates are highly sensitive to earthquake source characterization and modeling approaches. Similar variations have also been reported in tsunami modeling studies conducted along the southern coast of Java, where differences in rupture scenarios, bathymetric datasets, topographic representations, and numerical model configurations resulted in substantial differences in predicted inundation characteristics (Benazir and Oktari, 2024; Dias et al., 2024; Wulandani et al., 2024). These findings suggest that direct comparisons among studies should be interpreted carefully because tsunami inundation is controlled not only by earthquake magnitude but also by slip distribution, rupture geometry, source depth, and tsunami propagation directivity.

In the present study, a megathrust earthquake scenario based on the Widyantoro model with a maximum magnitude of Mw 8.8 and a multifault rupture configuration was implemented. Although the earthquake magnitude is comparable to that adopted in previous studies, the resulting tsunami characteristics differed due to variations in the spatial distribution of vertical seafloor deformation and the direction of tsunami energy propagation toward the coastline. Consequently, the concentration of tsunami energy reaching the Soge Beach and Taman Ngadirojo Beach sectors was lower than that reported in several previous modeling studies, resulting in reduced inundation distances and run-up heights. Similar observations have been reported by Pakoksung et al. (2023) and Yamanaka et al. (2023), who demonstrated that local coastal morphology and tsunami wave directivity can significantly influence the spatial distribution of tsunami impacts even under comparable earthquake magnitudes.

Another important factor contributing to these differences is the representation of coastal topography and land-surface characteristics. Unlike previous studies that primarily relied on conventional DEM products, this study employed a high-resolution terrain model derived from the integration of FABDEM and DeltaDTM. The improved terrain representation enabled the identification of micro-topographic features such as coastal ridges, drainage channels, natural embankments, and subtle elevation variations that can significantly influence tsunami flow pathways and inundation processes. Recent studies have demonstrated that the incorporation of high-resolution topographic data substantially improves the realism of tsunami inundation modeling and reduces the overestimation of inundation extent in low-relief coastal environments (Chen et al., 2023; Cheng et al., 2023; Dias et al., 2024).

Furthermore, this study incorporated land-cover-based Manning's roughness coefficients to represent variations in surface resistance associated with vegetation, built-up areas, agricultural land, and aquaculture ponds. The inclusion of spatially distributed roughness coefficients increased energy dissipation during overland flow and limited inland tsunami propagation. Similar findings have been reported by Bricker et al. (2015) and Cárdenas and Catalán (2022), who demonstrated that roughness parameterization may reduce tsunami inundation distances by approximately 10–40%, particularly in areas characterized by dense vegetation or urban development. The importance of incorporating surface friction effects has also been highlighted in recent tsunami modelling studies, which showed that roughness representation can significantly influence inundation extent, flow velocity, and run-up estimates (Chen et al., 2023). Therefore, the lower inundation and run-up values obtained in this study compared with previous studies may be partly associated with differences in roughness parameterization and its influence on tsunami energy dissipation during overland flow.

In addition to surface roughness, terrain representation also played an important role in controlling the simulated tsunami impacts. The integration of FABDEM and DeltaDTM provided a representation of coastal terrain conditions that differs from those adopted in previous studies, potentially contributing to variations in simulated inundation extent and run-up estimates. This influence is particularly relevant in Ngadirojo Subdistrict, where low-lying coastal plains, estuarine systems, and heterogeneous topographic conditions strongly control tsunami flow pathways. Small variations in elevation may alter inundation patterns, modify run-up characteristics, and influence the inland penetration of tsunami waves. Similar observations have been reported by Pakoksung et al. (2023), who demonstrated that coastal morphology and estuarine systems play a critical role in controlling tsunami amplification and inundation patterns. Likewise, Cheng et al. (2023) emphasized that terrain representation is an important factor influencing local-scale tsunami inundation modelling. Consequently, the differences between the results obtained in this study and those reported in previous investigations highlight the sensitivity of tsunami simulations to terrain representation and roughness parameterization. These findings underscore the importance of carefully considering both topographic datasets and surface resistance parameters when conducting local-scale tsunami hazard assessments in coastal regions of southern Java (Benazir & Oktari, 2024; Dias et al., 2024; Wulandani et al., 2024).

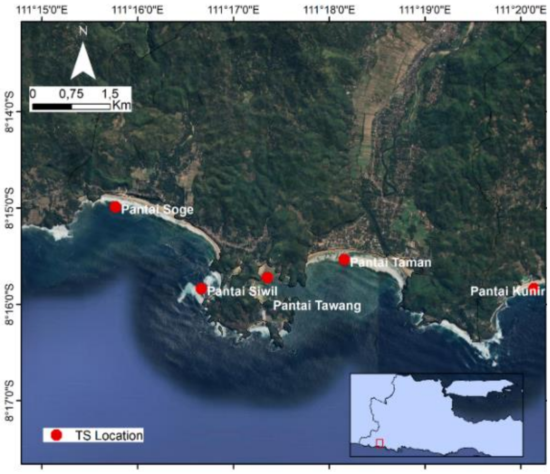

Figure 10. Virtual tide gauge observation point

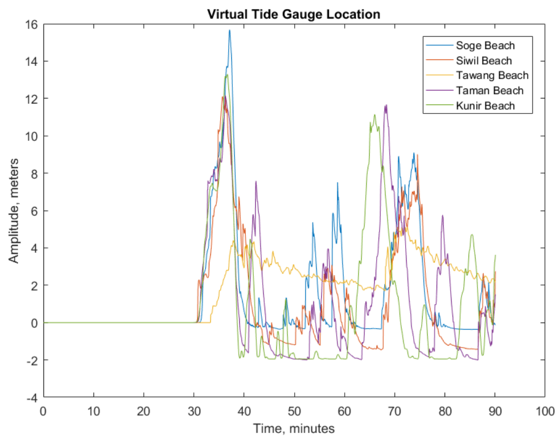

Figure 11. Tsunami arrival time at several monitoring points

3.3 Tsunami Hazard Level

The transformation of tsunami inundation modeling results into a tsunami hazard index was conducted as an intermediate step in the development of a tsunami hazard map. Although the COMCOT model generated quantitative parameters, including tsunami inundation, run-up, and arrival time, these outputs remain difficult to interpret directly for disaster mitigation and decision-making purposes. Therefore, tsunami inundation values were transformed into hazard indices ranging from 0 to 1 using a fuzzy logic approach. Within this framework, index values approaching 0 represent low hazard conditions, whereas values approaching 1 indicate high hazard conditions. The hazard index provides a standardized representation of continuous inundation data, thereby facilitating hazard classification and spatial interpretation. The spatial distribution of the tsunami hazard index in Ngadirojo Subdistrict is presented in Figure 12.

Subsequently, the hazard index was classified into three hazard classes, namely low, medium, and high hazard, based on the criteria established in the Indonesian National Disaster Management Agency (BNPB) Regulation No. 2 of 2012. This classification was intended to convert technical modeling outputs into operational spatial information that can be more readily utilized by decision-makers and other stakeholders. The resulting tsunami hazard map provides a practical basis for evacuation route planning, early warning system development, disaster-risk-informed spatial planning, and the prioritization of mitigation measures in areas with the highest levels of tsunami threat. Similar approaches have been widely applied in tsunami hazard assessment studies because they enable numerical modeling results to be translated into information that is more applicable for disaster risk reduction (Suppasri et al., 2019; Ibrahim et al., 2023). The spatial distribution of tsunami hazard classes in Ngadirojo Subdistrict is shown in Figure 13.

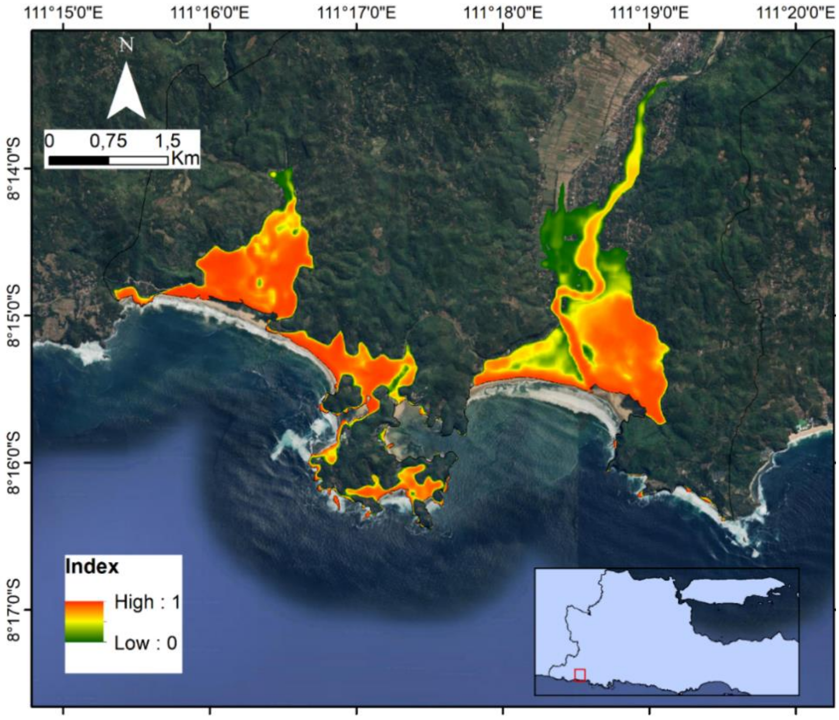

Figure 12. Tsunami hazard index map in Ngadirojo Subdistrict.

Based on the hazard classification results, the tsunami-affected area in Ngadirojo Subdistrict was divided into three hazard classes. Low-hazard areas covered 125.67 ha, medium-hazard areas covered 112.40 ha, and high-hazard areas covered 339.87 ha, resulting in a total affected area of approximately 577.94 ha (Table 4). High-hazard areas accounted for approximately 58.8% of the total inundated area, indicating that a substantial proportion of the exposed region is likely to experience severe impacts under the simulated tsunami scenario. The predominance of the high-hazard class highlights the significant tsunami threat facing the coastal areas of Ngadirojo Subdistrict and underscores the need for enhanced mitigation planning and community preparedness measures.

The spatial distribution of tsunami hazards reveals that high-hazard zones are concentrated along the coastal areas of Ngadirojo Subdistrict, particularly around Soge Beach and Taman Ngadirojo Beach. These areas are characterized by relatively gentle topography and interconnected estuarine systems, which facilitate deeper inland penetration of tsunami waves and result in more extensive inundation. In contrast, areas with higher elevations and steeper slopes generally experience more limited inundation impacts despite recording relatively high run-up values. These findings demonstrate that coastal morphology, coastal topography, and estuarine systems play important roles in controlling the spatial distribution of tsunami hazards in coastal environments (Benazir & Oktari, 2024; Wulandani et al., 2024).

Furthermore, the presence of semi-enclosed bays and river mouths contributes to increased tsunami hazard levels through wave refraction, resonance, and the channeling of tsunami flows toward inland areas. River mouths act as natural pathways that facilitate the propagation of tsunami waves into residential areas and agricultural land, while bay morphology promotes wave energy concentration and localized tsunami amplification. These findings are consistent with the studies of Pakoksung et al. (2023) and Dias et al. (2024), which demonstrated that estuarine environments, semi-enclosed bays, and low-lying coastal plains are generally associated with higher tsunami amplification and vulnerability than regions characterized by steeper topography. Similar observations were reported by Suppasri et al. (2019), who identified coastal geomorphology as one of the primary controls on tsunami inundation patterns and impact distribution in coastal regions.

The resulting tsunami hazard map has important implications for disaster mitigation efforts in Ngadirojo Subdistrict. Areas classified as high hazard should be prioritized for evacuation infrastructure development, early warning system enhancement, and community preparedness programs because they possess greater inundation potential and limited response time. The integration of high-resolution numerical modeling and spatial analysis enables the identification of priority mitigation areas with greater spatial detail, thereby supporting more effective disaster risk reduction strategies in coastal regions. This finding is consistent with Ibrahim et al. (2023), who emphasized the importance of high-resolution tsunami modeling in supporting evacuation planning and mitigation strategies in tsunami-prone coastal areas.

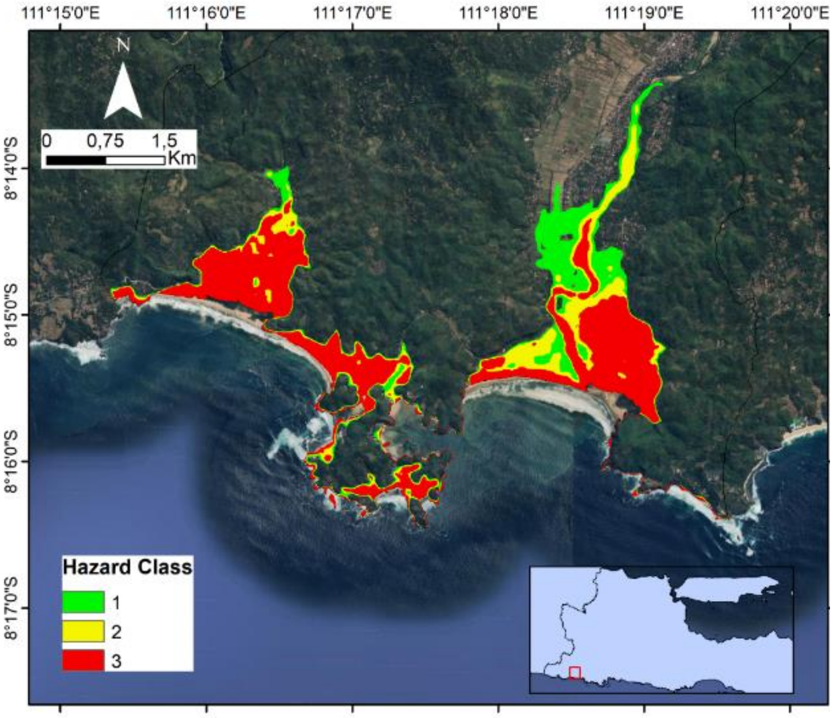

Figure 13. Tsunami hazard map in Ngadirojo Subdistrict.

The tsunami hazard map presented in Figure 13 indicates that Ngadirojo Subdistrict, particularly the coastal areas surrounding Soge Beach and Taman Ngadirojo Beach, constitutes a priority area for tsunami disaster risk management. These results confirm previous findings from studies conducted along the southern coast of Java (Dias et al., 2024) while further demonstrating the influence of bay morphology and estuarine systems on the spatial distribution of tsunami hazards at the local scale.

The spatial distribution of hazard classes reveals that high-hazard areas (Class 3) are concentrated along the coastal plains of Soge Beach and Taman Ngadirojo Beach, where low elevations and relatively gentle topography facilitate extensive tsunami inundation. In several locations, high-hazard zones extend inland through river-mouth and estuarine systems, indicating that these geomorphological features act as natural pathways that enhance tsunami penetration into coastal lowlands. Medium-hazard areas (Class 2) generally occur as transitional zones surrounding the high-hazard regions, reflecting the gradual reduction of tsunami energy as waves propagate inland. Meanwhile, low-hazard areas (Class 1) are primarily distributed farther inland and along the upper reaches of estuarine corridors, where increasing elevation and terrain resistance contribute to reducing tsunami inundation intensity.

A notable characteristic of the hazard map is the contrast between the locations of maximum run-up and maximum inundation extent. Although the highest run-up values were recorded at Soge Beach due to wave amplification associated with its embayed coastal morphology, the longest inundation distance occurred in the Taman Ngadirojo area, where low-relief topography and interconnected estuarine systems enabled tsunami flows to propagate farther inland. This finding highlights the distinct roles of coastal morphology and topography in controlling tsunami impacts and demonstrates that areas experiencing the highest run-up do not necessarily coincide with those experiencing the greatest inundation extent (Pakoksung et al., 2023; Yamanaka et al., 2023).

The dominance of high-hazard zones indicates that a substantial portion of the coastal area remains highly exposed to tsunami impacts. Therefore, the tsunami hazard map developed in this study provides a scientific basis for disaster risk reduction policies, evacuation planning, sustainable coastal development, and efforts to strengthen community resilience against future tsunami events.

Table 4. Total area hazard every cclassification in Ngadirojo Subdistrict.

Area	Low (Ha)	Medium (Ha)	High (Ha)
Ngadirojo	125.67	112.40	339.87

7. Conclusion

This study demonstrates that the coastal area of Ngadirojo Subdistrict, Pacitan Regency, is highly vulnerable to tsunami hazards generated by a potential Mw 8.8 South Java Megathrust earthquake. Numerical simulations using COMCOT reveal that tsunami waves can reach heights exceeding 16 m, with inundation penetrating nearly 4 km inland within approximately 30 minutes of wave arrival. The spatial distribution of hazard levels is strongly controlled by coastal morphology, where bay environments and river mouths amplify inundation, while low-lying plains facilitate deeper inland penetration. Conversely, steeper coasts record higher run-up but more localized flooding. The tsunami hazard index confirms that large portions of the study area, particularly Soge and Taman Ngadirojo Beaches, fall into high-risk categories. These results emphasize the urgent need for effective early warning systems, evacuation route planning, and risk-based spatial development. Moreover, the findings contribute valuable scientific evidence for disaster risk reduction strategies in tsunami-prone regions of Indonesia and the broader Indo-Pacific

Acknowledgements

The authors would like to express their sincere gratitude to the Center for Research and Community Development of the Shipbuilding Institute of Polytechnic Surabaya (PPNS) for providing financial support for this research. The authors also gratefully acknowledge Badan Informasi Geospasial, Badan Nasional Penanggulangan Bencana, and Badan Meteorologi, Klimatologi, dan Geofisika for their valuable support and provision of data used in this study.

References

Aditama, F. Y., Widodo, A., Rochman, J. P. G. N., & Pribadi, S. (2023). Pemodelan tsunami di Kecamatan Pacitan dan Kecamatan Ngadirojo Kabupaten Pacitan Jawa Timur. *Jurnal Geosaintek*, 9(3), 142–150. http://dx.doi.org/10.12962/j25023659.v9i3.18056

Anugrah, S. D., Zaim, Y., Rizal, Y., Aswan, & Istiyanati. (2015). A preliminary study of paleotsunami deposit along the south coast of East Java: Pacitan-Banyuwangi. *AIP Conference Proceedings*, 1658(1), 50003. https://doi.org/10.1063/1.4915251.

Ar, E., Hadmoko, D., & Widartono, B. (2025). Tsunami inundation modeling using high resolution uav-dem in a part of the coastal areas of bengkulu city. *IOP Conference Series Earth and Environmental Science*, 1503(1), 012022. https://doi.org/10.1088/1755-1315/1503/1/012022

Arafat, Y., Tunas, I. G., & Hidaya, N. (2025). Modelling the impact of sea level rise on ocean hydrodynamics: A case study of Tambu Bay. Mathematical Modelling of Engineering Problems, 12(2), 367–377.

Badan Nasional Penanggulangan Bencana. (2018). *Modul teknis penyusunan kajian risiko bencana tsunami (Versi 1.0)*. Direktorat Pengurangan Risiko Bencana, BNPB.

Budiman, M. J., Sutoyo, & Syafiudin, M. F. (2024). Pemetaan Kerentanan Bahaya Tsunami dengan Pemodelan Inundansi (Studi Kasus : Kabupaten Bantul). *Jurnal Teknik Sipil Dan Lingkungan*, 9(2), 157–166. https://doi.org/10.29244/jsil.9.2.157-166.

Cárdenas, G., & Catalán, P. A. (2022). Accelerating Tsunami Modeling for Evacuation Studies through Modification of the Manning Roughness Values. *GeoHazards*, 3(4), 492–507. https://doi.org/10.3390/geohazards3040025.

Cheng, A. C., Suppasri, A., Pakoksung, K., & Imamura, F. (2023). Resonance characteristics and impact of the 2006 Pingtung tsunami in southern. *Geoscience Letters*. https://doi.org/10.1186/s40562-023-00271-0

Dias, N., Haigh, R., Amaratunga, D., & Rahayu, H. (2024). A review of tsunami early warning at the local level - Key actors, dissemination pathways, and remaining challenges. *International Journal of Disaster Risk Reduction*, 101(December 2023), 104195. https://doi.org/10.1016/j.ijdrr.2023.104195.

Glimsdal, S., Pedersen, G. K., Harbitz, C. B., & Løvholt, F. (2013). Dispersion of tsunamis: does it really matter? *Natural Hazards and Earth System Sciences*, 13, 1507–1526. https://doi.org/10.5194/nhess-13-1507-2013

Handayani, W., Mutaqin, B. W., Marfai, M. A., Tyas, D. W., Alwi, M., Rosaji, F. S. C., Hilmansyah, A. A., Musthofa, A., & Fahmi, M. S. I. (2022). Coastal Hazard Modeling in Indonesia Small Island: Case Study of Ternate Island. *IOP Conference Series: Earth and Environmental Science*, 1039(1). https://doi.org/10.1088/1755-1315/1039/1/012025

Hamzah, L., Puspito, N. T., & Imamura, F. (2000). Tsunami Catalog and Zones in Indonesia. *Journal of Natural Disaster Science*, 22(1), 25–43. https://doi.org/10.2328/jnds.22.25

Horspool, N., Pranantyo, I., Griffin, J., Latief, H., Natawidjaja, D. H., Kongko, W., Cipta, A., Bustaman, B., Anugrah, S. D., & Thio, H. K. (2014). A probabilistic tsunami hazard assessment for Indonesia. *Natural Hazards and Earth System Sciences*, 14(11), 3105–3122. https://doi.org/10.5194/nhess-14-3105-2014.

Ibrahim, Syamsidik, Azmeri, Hasan, M., Irwansyah, A., & Al Farizi, M. D. (2023). Assessing tsunami vertical evacuation processes based on probabilistic tsunami hazard assessment for west coast of Aceh Besar, Indonesia. *Geoenvironmental Disasters*, 10(1). https://doi.org/10.1186/s40677-023-00238-5

Jumadi, J., Priyono, K. D., Amin, C., Saputra, A., Gomez, C., Lam, K.-C., Rohman, A., Patel, N., Sattar, F., & Nawaz, M. (2025). Tsunami risk mapping and sustainable mitigation strategies for megathrust earthquake scenario in Pacitan coastal areas, Indonesia. *Sustainability*, 17(6), 2564. https://doi.org/10.3390/su17062564

Kaiser, G., Scheele, L., Kortenhaus, A., Løvholt, F., Römer, H., & Leschka, S. (2011). The influence of land cover roughness on the results of high resolution tsunami inundation modeling. *Natural Hazards and Earth System Science*, 11(9), 2521–2540. https://doi.org/10.5194/nhess-11-2521-2011.

Li, K., Salmanidou, D., Gopinathan, D., Heidarzadeh, M., & Guillas, S. (2025). Uncertainty in

Manning's roughness coefficient in multilevel simulations of future tsunamis in Sumatra. Proceedings of the Royal Society A: Mathematical, *Physical and Engineering Sciences*, 481(2316). https://doi.org/10.1098/rspa.2024.0637

Marsh, C. B., Harder, P., & Pomeroy, J. W. (2023). Validation of FABDEM, a global bare-earth elevation model, against UAV-lidar derived elevation in a complex forested mountain catchment. *Environmental Research Communications*, 5(3). https://doi.org/10.1088/2515-7620/acc56dhttps://doi.org/10.3390/su17062564.

Merz, B., Kuhlicke, C., Kunz, M., Pittore, M., Babeyko, A., Bresch, D. N., et al. (2020). Impact forecasting to support emergency management of natural hazards. *Reviews of Geophysics*, 58, e2020RG000704. https://doi.org/ 10.1029/2020RG000704.

Núñez, J., Catalán, P. A., Valle, C., Zamora, N., & Valderrama, A. (2022). Discriminating the occurrence of inundation in tsunami early warning with one - dimensional convolutional neural networks. *Scientific Reports*, 1–20. https://doi.org/10.1038/s41598-022-13788-9

Okal, E. A., & Synolakis, C. E. (2008). Far-field tsunami hazard from mega-thrust earthquakes in the Indian Ocean. *Geophysical Journal International,* 172(3), 995–1015. https://doi.org/10.1111/j.1365-246X.2007.03674.x

Osama, N., Shao, Z., & Freeshah, M. (2023). The FABDEM Outperforms the Global DEMs in Representing Bare Terrain Heights. *Photogrammetric Engineering and Remote Sensing*, 89(10), 613–624. https://doi.org/10.14358/PERS.23-00026R2.

Pakoksung, K., Suppasri, A., & Imamura, F. (2023). Resonance characteristics of tsunami in bay of Japan by the Hunga Tonga - Hunga Ha ' apai volcano eruption on 15th January. *Scientific Reports*, 1–16. https://doi.org/10.1038/s41598-023-45601-6.

Panguale, M. R., Hamka, M. S. R., Dinata, S. M., Arsalia, R., Nabila, A. N., Febrianti, S., & Agustina, N. A. A. D. (2025). Pemetaan tingkat bahaya tsunami menggunakan sistem informasi geografis di Kabupaten Trenggalek. *Seminar Nasional Terapan Riset Inovatif (SENTRINOV)*: Seri Engineering and Science, 11(1), 431–446.

Pribadi, S., Kongko, W., Rahili, N., Fauzi, F., Suntoko, H., Nugroho, S., & Alhakim, E. (2023). Assessing the potential tsunami source of the manila trench at the bengkayang nuclear power plant site in kalimantan using topographical details. *International Journal of Renewable Energy Development*, 13(1), 158-167. https://doi.org/10.14710/ijred.2024.57967.

Pronk, M., Hooijer, A., Eilander, D., Haag, A., de Jong, T., Vousdoukas, M., Vernimmen, R., Ledoux, H., & Eleveld, M. (2024). DeltaDTM: A global coastal digital terrain model. *Scientific Data*, 11(1), 1–18. https://doi.org/10.1038/s41597-024-03091-9.

Rina, B., & Oktari, S. (2024). Assessing tsunami risk along the Aceh coast , Indonesia : a quantitative analysis of fault rupture potential and early warning system efficacy for predicting arrival time and flood extent. *Natural Hazards*, 120(5), 4875–4900. https://doi.org/10.1007/s11069-024-06401-x.

Saito, T. (2013). Dynamic tsunami generation due to sea-bottom deformation: Analytical representation based on linear potential theory. *Earth Planets Space*, 65, 1411–1423. https://doi.org/10.5047/eps.2013.07.004

Satake, K. (2014). Advances in earthquake and tsunami sciences and disaster risk reduction since the 2004 Indian ocean tsunami. *Geoscience Letters*, 15(1). https://doi.org/10.1186/s40562-014-0015-7.

Setyaningsih, D. P., Sutiono, H. E. C. P., Paramanandi, A. R. G., Khasanah, E. U., Wahyuni, T., Jati, B. A. E. K., Akbar, M. F. Al, Widyatmanti, W., & Wibowo, T. W. (2023). Tsunami Hazard Modeling in the Coastal Area of Kulon Progo Regency. *International Journal of Remote Sensing and Earth Sciences*, 19(2), 184. https://doi.org/10.30536/j.ijreses.2022.v19.a3822.

Supendi, P., Widiyantoro, S., Rawlinson, N., Yatimantoro, T., Muhari, A., Hanifa, N. R., Gunawan, E., Shiddiqi, H. A., Imran, I., Anugrah, S. D., Daryono, D., Prayitno, B. S., Adi, S. P., Karnawati, D., Faizal, L., & Damanik, R. (2023). On the potential for megathrust earthquakes and tsunamis off the southern coast of West Java and southeast Sumatra, Indonesia. *Natural Hazards*, 116(1), 1315–1328. https://doi.org/10.1007/s11069-022-05696-y

Tonegawa, T., & Fukao, Y. (2022). Wave propagation of meteotsunamis and generation of free tsunamis in the sloping area of the Japan Trench for the 2022 Hunga – Tonga volcanic eruption. *Earth, Planets and Space*, 74(156). https://doi.org/10.1186/s40623-022-01727-x

Triyono, R., Prasetya, T., Anugrah, S. D., Sudrajat, A., Setiyono, U., Gunawan, I., Priyobudi, Yatimantoro, T., Hidayanti, Anggraini, S., Rahayu, R. H., Yogaswara, D. S., Hawati, P., Apriyani, M., Julius, A. M., Harvan, M., Simangunsong, G., & Kriswinarso, T. (2019). Katalog Tsunami Indonesia Per-Wilayah Tahun 416-2018. In Pusat Gempabumi dan Tsunami Kedeputian Bidang Geofisika.

Wang, W., & Power, W. L. (2011). COMCOT: A tsunami generation, propagation and run-up model. GNS Science. ISBN 9780478198676.

Wibowo, Y. A., Subadi, T., Wardhani, P. I., Syahputri, D. M., Hidayah, K., Sholikah, S. N. H., & Ronggowulan, L. (2023). Geospatial technology-based tsunami-prone areas identification, Pacitan, Indonesia. *AIP Conference Proceedings*, 2683(1), 30033. https://doi.org/10.1063/5.0125730

Widiyantoro, S., Gunawan, E., Muhari, A., Rawlinson, N., Mori, J., Hanifa, N. R., Susilo, S., Supendi, P., Shiddiqi, H. A., Nugraha, A. D., & Putra, H. E. (2020). Implications for megathrust earthquakes and tsunamis from seismic gaps south of Java Indonesia. *Scientific Reports*, 10(1), 1–11. https://doi.org/10.1038/s41598-020-72142-z.

Widodo, A., Aditama, F. Y., Rochman, J. P. G. N., Kartikasari, D., Putra, N. M., & Pribadi, S. (2024). Preliminary study of tsunami simulations on megathrust earthquake scenarios in Pacitan Regency, East Java. *IOP Conference Series: Earth and Environmental Science*, 1307(1), 0–10. https://doi.org/10.1088/1755-1315/1307/1/012004.

Windupranata, W., Al Ghifari, M. W., Nusantara, C. A. D. S., Shafa, M., Hayatiningsih, I., Mulia, I. E., & Nuraghnia, A. (2025). Probabilistic tsunami hazard analysis of Batukaras, a tourism village in Indonesia. *Natural Hazards and Earth System Sciences*, 25, 1057–1069. https://doi.org/10.5194/nhess-25-1057-2025.

Wulandani, N. A., Wibowo, Y. A., & Nurwijayanti, A. (2024). Identification of coastal typology and utilization of geospatial technology for tsunami hazard modeling in Kulon Progo coastal area, Special Region of Yogyakarta, Indonesia. *IOP Conference Series: Earth and Environmental Science*, 1357(1), 012040. https://doi.org/10.1088/1755-1315/1357/1/012040.

Yamanaka, Y., Hashimoto, K., & Tajima, Y. (2023). Real-time tsunami forecasting system with nonlinear effects using Green's functions: application to near-shore tsunami behavior in complex bay topography. *Coastal Engineering Journal*, 65(4), 546–559. https://doi.org/10.1080/21664250.2023.2278367

Yusdian, M., Prasetiyo, R., Supriyadi, A., & Prihanto, Y. (2023). Tsunami disaster modeling for non-military defense in pangandaran regency using geographic information systems. *International Journal of Remote Sensing and Earth Sciences (Ijreses)*, 20(1), 45. https://doi.org/10.30536/j.ijreses.2023.v20.a3842